Polymer Chemistry

ROYAL SOCIETY OF CHEMISTRY

PAPER

View Article Online
View Journal | View Issue

Published on 27 December 2023. Downloaded by National Sun Yat Sen University on 5/13/2024 10:20:48 AM.

Check for updates

Cite this: *Polym. Chem.*, 2024, **15**, 397

Bifunctional imidazolium linked tetraphenylethene based conjugated microporous polymers for dynamic antibacterial properties and supercapacitor electrodes†

Aya Osama Mousa,[a,b] Zheng-Ian Lin,[c] Swetha V. Chaganti,[d] Cheng-Hsin Chuang, *[b] Chih-Kuang Chen,*[c] Shiao-Wei Kuo *[a,e] and Mohamed Gamal Mohamed *[a,f]

Received 25th November 2023,
Accepted 23rd December 2023

DOI: 10.1039/d3py01303k

rsc.li/polymers

Conjugated microporous polymers (CMPs) present intriguing potential for a myriad of applications. In this study, we detail the synthesis of bimine-linked conjugated microporous polymers (CMPs), namely TPET-Bimine and PT-Bimine CMPs, through Sonogashira–Hagihara cross-coupling. The process involves coupling the (1*E*,2*E*)-N^1,N^2-bis(4-bromophenyl)ethane-1,2-diimine (Bimine-B_{r2}) building block with 1,1,2,2-tetrakis(4-ethynylphenyl)ethene (TPET) and 1,3,6,8-tetraethynylpyrene (PT) units, followed by partial post-cyclization into an imidazolium (Im)-linked CMP (TPET-Im and PT-Im CMPs). Our investigation covers thermal stability, molecular structure, porous characteristics, and potential applications of these novel CMPs using various analytical techniques. Notably, TPET-Bimine CMP demonstrates superior thermal stability (T_{d10} = 390 °C) with a char yield of 67 wt% and the highest BET surface area of 451 m^2 g^{-1} compared to the other samples. The antibacterial activities and electrochemical performance of all synthesized CMPs were assessed. Im-linked CMPs exhibited enhanced antibacterial activity and improved electrochemical capacitance compared to the pristine samples without the imidazolium ring. The cationic linkage facilitates a robust interaction with bacterial membranes, enhancing antibacterial efficacy, particularly against *Staphylococcus aureus* (*S. aureus*). Antibacterial activity increased with higher concentrations of Im-linked CMPs; for instance, PT-Im and TPET-Im CMPs showed the highest antibacterial activity at 15 mg mL^{-1}. Cytotoxicity evaluation against L929 fibroblasts demonstrated good compatibility in the presence of Im-linked CMPs. Additionally, TPET-Im CMP displayed the highest specific capacitance of 63 F g^{-1}, coupled with an energy density of 8.73 W h Kg^{-1} in supercapacitive studies. These results highlight the potential applications of Im-linked CMPs as both antibacterial agents and electrode materials for supercapacitors.

Introduction

Bacteria, omnipresent and thriving on seemingly inconceivable surfaces, establish a delicate balance between human life and the environment. Their prevalence holds significance, as many strains pose potential health risks, leading to the spread of dangerous illnesses.[1] The widespread and indiscriminate use of antibiotics, a vital tool in combating microorganisms and extending the human lifespan, has inadvertently given rise to antibiotic-resistant bacteria, complicating antimicrobial treatments.[2] Addressing the menace of antibiotic resistance is crucial, necessitating the exploration of alternative and effective antimicrobial materials.[2–6] A diverse range of synthetic antimicrobial agents has emerged to tackle this challenge, including antimicrobial polymers, cationic compounds, antimicrobial peptides, and inorganic antimicrobial

[a]*Department of Materials and Optoelectronic Science, Center of Crystal Research, National Sun Yat-Sen University, Kaohsiung 804, Taiwan. E-mail: kuosw@faculty.nsysu.edu.tw, mgamal.eldin12@yahoo.com*
[b]*Institute of Medical Science and Technology, College of Medicine, National Sun Yat-sen University, Kaohsiung 804201, Taiwan. E-mail: chchuang@imst.nsysu.edu.tw*
[c]*Polymeric Biomaterials Laboratory, Department of Materials and Optoelectronic Science, National Sun Yat-Sen University, Kaohsiung 804, Taiwan. E-mail: chihkuan@mail.nsysu.edu.tw*
[d]*Department of Chemistry, National Sun Yat-sen University, Kaohsiung 804, Taiwan*
[e]*Department of Medicinal and Applied Chemistry, Kaohsiung Medical University, Kaohsiung 807, Taiwan*
[f]*Chemistry Department, Faculty of Science, Assiut University, Assiut 71515, Egypt*
†Electronic supplementary information (ESI) available. See DOI: https://doi.org/10.1039/d3py01303k

Published on 27 December 2023. Downloaded by National Sun Yat Sen University on 5/13/2024 10:20:48 AM.

agents.[7–16] Among these, cationic polymers have garnered significant attention due to their heightened antibacterial efficacy and comparatively lower toxicity.[17,18] Currently, antimicrobial polymers based on pyridinium,[19] pyrrolidinium,[20] quaternary ammonium,[21] piperidinium,[22] and imidazolium[23,24] have been developed and employed in antibacterial applications. This growing focus on cationic polymers reflects their potential as promising solutions in the quest for effective and sustainable antimicrobial strategies.[25] Over the years, the health risks to both human and animal life have escalated. This increase is attributed not only to environmental pollution caused by harmful organisms but also to contaminants linked to the extensive use of fossil fuels.[26,27] This includes excessive carbon dioxide (CO_2) emissions and hazardous pollutants released from vehicle exhaust. To address the critical issue jeopardizing the ecosystem, scientists have directed their efforts toward intensifying research for the development of innovative, sustainable, and efficient alternatives in the realm of renewable energy storage.[28,29] One standout solution is the supercapacitor, known for its outstanding speed capabilities, safe operation, maximal capacity, environmentally friendly attributes, prolonged cycle stability, minimal fabrication cost, and high power density.[30–32] Supercapacitors (SCs) are categorized into electrochemical pseudocapacitors and electric double-layer capacitors (EDLCs) based on their charge-storing mechanisms.[33,34] Pseudocapacitors store energy through highly reversible redox interactions between electrolyte ions and electrode materials.[35] On the other hand, EDLCs primarily store energy at the electrode–electrolyte interface by adsorbing and desorbing charged ions.[36] The performance of supercapacitors is significantly influenced by the choice of materials for the electrodes. Traditionally, inorganic materials were extensively used in supercapacitors, but their environmental impact raised concerns.[37] To address these shortcomings and seek more sustainable alternatives, the development of polymers becomes pivotal for the advancement of supercapacitor technology.[38–40] Conjugated microporous polymers (CMPs) have captured significant scientific attention within the realm of porous materials due to their remarkably porous extended π-conjugated architecture.[41] What sets CMPs apart are distinctive features such as low toxicity, low structure density, and thermal stability, coupled with controlled assemblies facilitated by the principles of crystal engineering.[42] CMPs can be synthesized through various techniques, including Suzuki–Miyaura coupling, Sonogashira–Hagihara coupling, Buchwald–Hartwig amination, Yamamoto, and others.[43–45] The ability to incorporate rational functional modifications into the porous structure enhances CMPs' potential to address energy and environmental challenges, allowing for diverse applications. These applications span gas storage and separation, photo-catalysis, bioimaging, antibacterial treatments, biosensing, optoelectronic devices, dye adsorption, and drug delivery, showcasing the multifaceted capabilities of CMP frameworks.[46–51] Previous studies have underscored the efficacy of utilizing CMPs in both antibacterial applications and supercapacitors. Wang *et al.* devised a method to enhance the antibacterial properties of CMPs by introducing hydantoin groups, resulting in superior performance.[52] Lei *et al.* developed a novel CMP using acetylene and trichloroisocyanuric acid as monomer fragments, demonstrating the complete suppression of *E. coli* and *S. aureus* growth within 3 hours.[53] Wu *et al.* presented a technique for crafting CMP antibacterial compounds by introducing sulfur and nitrogen heteroatoms into the 1,10-phenanthroline framework, achieving a 100% mortality rate for *E. coli* within 12 hours.[54] Mousa *et al.* engineered a novel CMP named An-Ph-TPA CMP as an electrode material, showcasing a capacitance of 116 F g^{-1}.[55] Leveraging the advantages of CMPs, we synthesized bimine-linked CMPs, specifically PT-Bimine CMP and TPET-Bimine CMP, with a notable surface area through Sonogashira–Hagihara cross-couplings involving a newly synthesized Bimine-Br_2 and TPET and PT units. Subsequently, a subtle ring closure using chloromethyl ethyl ether enabled the transformation of adjustable bisimine links in PT-Bimine CMP and TPET-Bimine CMP into partly imidazolium (Im)-linked CMPs (PT-Im and TPET-Im CMPs). These Im-linked CMPs were then explored for their potential applications as antibacterial agents and supercapacitor electrode materials. The physicochemical and morphological attributes of the four synthesized CMPs—PT-Bimine CMP, TPET-Bimine CMP, PT-Im CMP, and TPET-Im CMP—were comprehensively characterized using various techniques such as FTIR, TGA, BET, XPS, SEM, NMR, and TEM. Among these, TPET-Bimine CMP exhibited superior thermal stability (T_{d10} = 390 °C) with a char yield of 67 wt% and the highest BET surface area of 451 m^2 g^{-1}. In antibacterial testing, Im-linked CMPs demonstrated potent antibacterial effects against *S. aureus*. Cytocompatibility assessments with L929 fibroblasts validated the ultralow toxicity of these CMPs. Additionally, we explored the practical application of these CMPs as supercapacitor electrode-active materials. The introduction of imidazolium groups, notably in TPET-Im CMP, resulted in high electrochemical performance, displaying a capacitance of 63 F g^{-1} considerably greater than that of TPET-Bimine CMP (capacitance of 34 F g^{-1}). Considering the superior antibacterial characteristics, minimal toxicity, and impressive electrochemical performance of our novel Im-linked CMPs, these materials showcase promise for diverse applications in fields such as antibacterial treatments and energy storage.

Experimental section

Materials

4-Bromoaniline, tetrahydrofuran (THF), triphenylphosphine (PPh_3, 99%), ethyl acetate, methanol (MeOH), triethylamine (Et_3N, 99.5%), chloromethyl ethyl ether, copper(I) iodide (CuI, 99%), glyoxal, acetone, tetrakis(triphenylphosphine)palladium [$Pd(PPh_3)_4$], and isopropyl alcohol were obtained from diverse commercial sources (Sigma-Aldrich, Alfa Aesar, J. T. Baker, Acros). As stated, in our previous research, we efficaciously prepared PT and TPET.[56–59]

 This journal is © The Royal Society of Chemistry 2024

Published on 27 December 2023. Downloaded by National Sun Yat Sen University on 5/13/2024 10:20:48 AM.

Synthesis of Bimine-Br_2

Glyoxal (6.4 mL, 139.49 mmol) was combined with isopropyl alcohol (50 mL) and stirred for nearly 15 minutes under ice-cooling (0 °C). Subsequently, a solution of 4-bromoaniline (15 g, 87.19 mmol) in isopropyl alcohol (100 mL) was slowly added dropwise using a syringe into a two-neck reaction flask. The resulting mixture was then swirled for 24 hours. Following this period, the product was filtered and thoroughly washed with isopropyl alcohol. Finally, the resulting residue was dried under vacuum, yielding a yellow powder. FTIR (Fig. S1†): 3045, 2925 (aliphatic C–H), 1606 (C═N), 653 (C–Br). ^{1}H NMR (Fig. S2†) δ 8.45 (s, 2H), 7.64 (d, 4H), 7.35 (d, 4H). ^{13}C NMR (Fig. S3†): 161.6, 149.2, 133.1, 123.8, 121.3. T_{d10} = 259 °C and char yield = 33 wt% (using TGA (Fig. S4†)).

Synthesis of TPET-Bimine CMP

CuI (0.011 g, 0.057 mmol), PPh_3 (0.015 g, 0.057 mmol), Pd $(PPh_3)_4$ (0.06 g, 0.052 mmol), TPE-T (0.25 g, 0.584 mmol), and Bimine-Br_2 (0.43 g, 1.174 mmol) were mixed in DMF (15 mL) and Et_3N (15 mL). The mixture was heated for 72 hours to 100 °C. After the reaction was finished, the orange precipitate that was produced was filtered out and thoroughly cleaned using THF, and MeOH. After that, the product was dried for a whole night at 80 °C, producing TPET-Bimine CMP (0.93 g, 84%).

Synthesis of PT-Bimine CMP

PPh_3 (0.022 g, 0.083 mmol), CuI (0.015 g, 0.078 mmol), PT (0.25 g, 0.837 mmol), Bimine-Br_2 (0.61 g, 1.674 mmol), Pd $(PPh_3)_4$ (0.05 g, 0.043 mmol), and Et_3N (15 mL) were mixed. After 72 hours of reflux heating, the mixture reached 100 °C. The dark precipitate was removed from the reaction by filtering it and giving it a thorough washing in THF, MeOH, and acetone once it had finished. A yield of 0.29 g (84%), was obtained by drying it overnight.

Synthesis of TPET-Im and PT-Im CMPs

In an inert atmosphere, TPET-Bimine CMP (0.3 g) or PT-Bimine CMP (0.2 g), along with chloromethyl ethyl ether (0.2 mL) and THF (15 mL), were introduced into an oven-dried flask. The flask gently swirled for two days while maintaining a temperature of 40 °C. After isolating the resulting solid through filtration, it was washed with anhydrous ethyl acetate and subsequently vacuum-dried. This process yielded TPET-Im CMP as a dark amber solid and PT-Im CMP as a dark brown solid.

Antibacterial activity evaluation of bimine-linked CMPs and Im-linked CMPs

In this research, *S. aureus* (ATCC No. 25923) was cultivated using agar/broth media at 37 °C. The microorganisms were diluted in phosphate-buffered saline (PBS) solution to a concentration of 3×10^8 CFU mL^{-1} upon reaching the mid-logarithmic stage. Subsequently, PT-Bimine, PT-Im, TPET-Bimine, and TPET-Im CMPs were introduced to centrifuge tubes at concentrations ranging from 5–15 mg mL^{-1}. To each centrifuge tube, 1 mL of microbial suspension was added and incubated at a constant temperature for 18 hours. Following the incubation, a 10^{-1}–10^{-6}-fold dilution was performed on 100 μL of the mixture. Finally, 5 μL of the diluted solution was added dropwise to pre-prepared agar plates, with 2 drops applied for each dilution as shown in Fig. S5,† before incubating at 37 °C for 18 hours. The resultant microbial colonies were then documented through photography. As an alternative approach for SEM analysis, the cultured bacterial solution underwent centrifugation and fixation using a 2.5% glutaraldehyde solution for 4 h. Subsequently, the bacteria were subjected to two washes with PBS. The solution was then dehydrated through sequential immersions in aqueous ethanol with gradient concentrations (30%, 50%, 70%, 90%, 95%, and 100%), with each concentration having an immersion time of 15 minutes. The bacterial solution was applied onto slides and allowed to air-dry for 2 days at room temperature. Following this, gold was evaporated onto the slide's surface, and SEM observations were conducted using a SU-5000 microscope from HITACHI at an acceleration voltage of 15 kV.

Cytocompatibility test of bimine-linked CMPs and Im-linked CMPs

In this investigation, L929 fibroblasts were employed to evaluate the impact of CMPs on biotoxicity and L929 proliferation. The MTT colorimetric assay, aligned with the ISO 10993-5 test method, was employed. Initially, 5 mg mL^{-1} of CMPs were introduced into an L929 fibroblast solution and incubated at 37 °C for 48 hours. The initial concentration of L929 fibroblasts in 96-well plates was 5 × 103 cells per well, and the cells were cultured at 37 °C/5% CO_2. Following the completion of the cell culture, the media was aspirated from the 96-well plates, and the cells were rinsed with pH 7.4 PBS. Subsequently, the culture media was once again removed after incubation, and the 96-well plate was washed with a pH 7.4 PBS solution. The plate was then placed in an incubator at 37 °C/5% CO_2 for 4 hours following the addition of 10 μL of MTT solution (1 mg mL^{-1} in MEM) to each well. Following incubation, the media was withdrawn, and 70 μL of DMSO was added to each well to dissolve the MTT reaction product that had formed. Subsequently, the plate underwent vigorous shaking for 15 minutes to ensure thorough mixing of DMSO and the reaction product. Optical densities at 570 nm were then detected using a Microplate Reader (800TS/BioTek), with 630 nm serving as the reference wavelength. The optical densities of the remaining test samples were quantified as a percentage of cell viability relative to the optical density of samples lacking CMP. The optical density of L929 cells without samples was established as the standard (100%). The results for cell viability were obtained from three independent trials. Furthermore, optical microscopy was employed to examine the adhesion and proliferation characteristics of CMPs. The initial step included the removal of the CMP culture medium, followed by washing the tray's bottom with phosphate buffer solution (PBS; pH = 7.4) to eliminate any

Published on 27 December 2023. Downloaded by National Sun Yat Sen University on 5/13/2024 10:20:48 AM.

dead cells. Subsequently, images of L929 fibroblasts were observed using an optical microscope (BX51/Olympus).

Results and discussion

The synthesis of imidazolium (Im)-linked CMP frameworks involved a three-step process. Initially, a novel Bimine-Br_2 monomer was easily prepared by condensing glyoxal and 4-bromoaniline in isopropyl alcohol at 0 °C (Scheme S1†). Subsequently, bimine-linked CMPs (TPET-Bimine [Scheme S2†] and PT-Bimine [Scheme S3†] CMPs) were synthesized through Sonogashira couplings of Bimine-Br_2 with TPET and PT units in a 1 : 1 mixture of DMF and Et_3N, employing a palladium catalyst (Fig. 1(a) and (b)). Finally, the Im-linked CMPs [Fig. 1(c), (d) and Schemes S4, S5†] were obtained in good yield by reacting the bimine-linked CMPs with chloromethyl ethyl ether as a mild reagent to close the ring in THF at 40 °C for 2 days. The resulting CMPs were insoluble and stable in water and most typical solvents, indicating high chemical stability and well-crosslinked networks. The chemical structures of the novel Bimine-Br_2 monomer and these four CMPs were initially confirmed using FTIR and NMR spectroscopy. The FTIR spectrum of Bimine-Br_2 lacked the C=O characteristic peak for glyoxal and NH_2 characteristic peak for 4-bromoaniline but displayed new absorption bands at 1606 cm^{-1}, attributed to the emerging C=N linkage (Fig. S1†). Bimine-Br_2 exhibited additional absorption bands at 653 cm^{-1} for C–Br and 3045 cm^{-1} for aromatic C–H. In the ^1H NMR spectrum of Bimine-Br_2, two doublets were observed at 7.64 and 7.35 ppm, corresponding to the aromatic protons, along with a singlet at 8.45 ppm, attributed to the –N=CH– (imine group) protons (Fig. S2†). As depicted in Fig. 2(a), FTIR spectra provided evidence for the presence of alkyne linkers in all the resulting CMPs, as indicated by the appearance of a stretching absorption band for –C≡C– bonds at 2182 cm^{-1}.

Additionally, absorption bands at 3073–3062 and 1627 cm^{-1} were observed in the FTIR spectra of all CMPs, signifying the stretching of aromatic C–H and C=N units. The distinctive alkyne C–H peak from TPET and PT disappeared, indicating the successful coupling of Bimine-Br_2 with TPET and PT units *via* the Sonogashira reaction. Further validation of the chemical structures of bimine-linked CMPs and Im-linked CMPs was carried out using solid-state ^{13}C NMR [Fig. 2(b)]. In the solid-state ^{13}C NMR spectrum of TPET-Bimine, PT-Bimine, TPET-Im, and PT-Im CMPs, signals of aromatic carbon were observed in the range of 110 to 150 ppm, and a distinct imine carbon peak was discernible at 179.92 ppm. Additionally, the signal of the alkyne groups in these frameworks was observed at 82 ppm, providing further evidence of complete monomer polymerization. TGA of synthesized TPET-Bimine, PT-Bimine, TPET-Im, and PT-Im CMPs, conducted under N_2 from 40 °C to 800 °C, demonstrated the high thermostability of these CMPs. The 10% weight losses for TPET-Bimine, PT-Bimine, TPET-Im, and PT-Im CMPs occurred at 390, 342, 365, and 354 °C, respectively, with char yields of 67, 66, 61, and 62 wt% after heating to 800 °C [Fig. 2(c)]. Elemental compositions of the bimine-linked CMPs and Im-

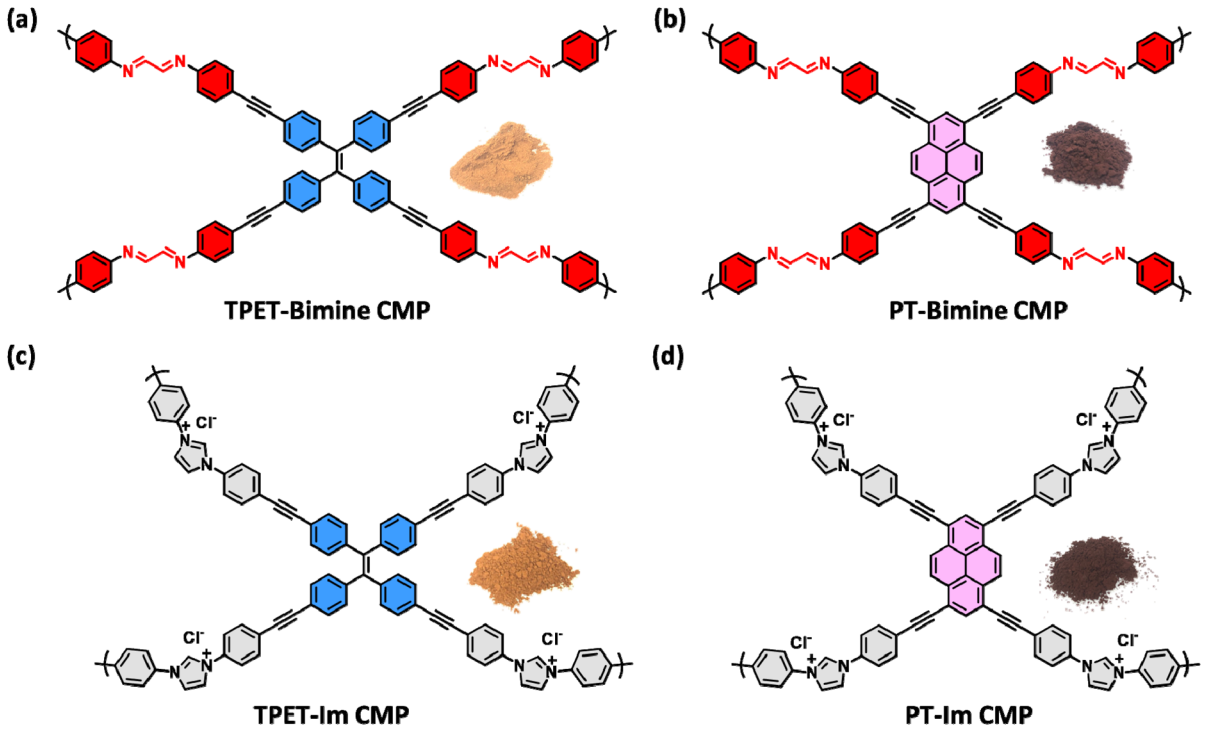

Fig. 1 The chemical structures of (a) TPET-Bimine CMP, (b) PT-Bimine CMP, (c) TPET-Im CMP and (d) PT-Im CMP.

 This journal is © The Royal Society of Chemistry 2024

Published on 27 December 2023. Downloaded by National Sun Yat Sen University on 5/13/2024 10:20:48 AM.

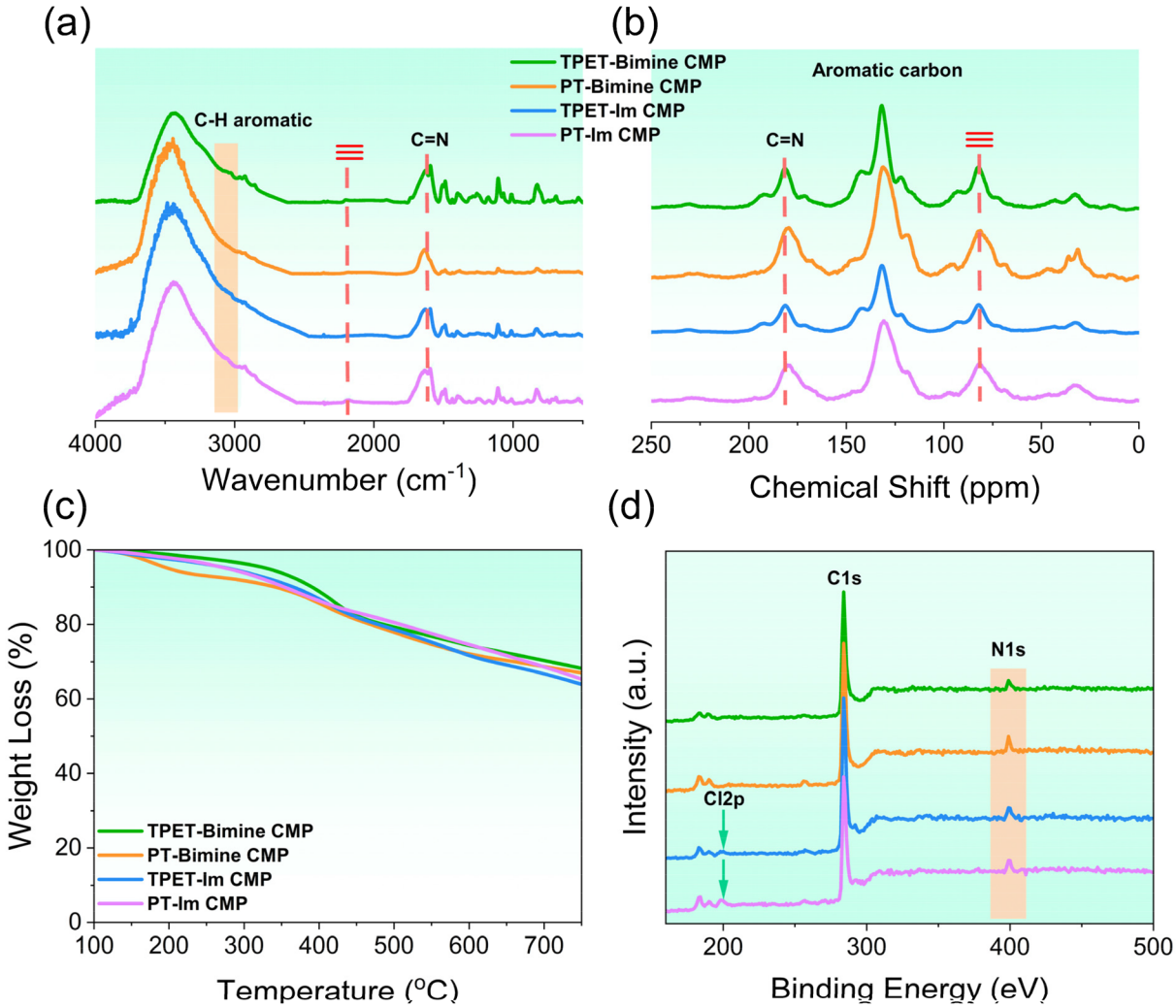

Fig. 2 (a) FTIR, (b) solid state ^{13}C NMR, (c) TGA and (d) XPS of TPET-Bimine CMP, PT-Bimine CMP, TPET-Im CMP and PT-Im CMP.

linked CMPs were estimated using XPS. The results confirmed the presence of carbon (C) and nitrogen (N) elements in TPET-Bimine, PT-Bimine, TPET-Im, and PT-Im CMP frameworks. Additionally, the Cl element was found in both TPET-Im and PT-Im CMPs [Fig. 2(d)]. The porous characteristics of the synthesized CMPs were evaluated through nitrogen adsorption/desorption analyses at 77 K [Fig. 3(a–h)]. The N_2 isotherm profiles of TPET-Bimine, PT-Bimine, and TPET-Im CMPs exhibited a combination of Type I and Type IV isotherms, while PT-Im CMP displayed a Type III isotherm as per the IUPAC classification. The sorption isotherms of TPET-Bimine, PT-Bimine, and TPET-Im CMPs indicated an increase in uptake at low relative pressures (<0.1), indicating the presence of a substantial number of micropores. Subsequently, N_2 adsorption increased at relative pressures (P/P_0) between 0.1 and 0.8. Moreover, at P/P_0 of 0.8, both N_2 isotherms showed consistent nitrogen uptakes, suggesting the coexistence of macropores and mesopores in these three CMP networks. The Brunauer–Emmett–Teller (BET) surface areas and total pore volumes of bimine-linked CMPs were determined as 451 $m^2\ g^{-1}$ and 0.61 $cm^3\ g^{-1}$ for TPET-Bimine CMP and 155 $m^2\ g^{-1}$ and 0.21 $cm^3\ g^{-1}$ for PT-Bimine CMP, respectively. Post-cyclization significantly affected the porosity of bimine-linked CMPs, with the BET surface area of TPET-Im and PT-Im CMPs reduced to 330 and 16.1 $m^2\ g^{-1}$, along with total pore volumes of 0.52 and 0.08 $cm^3\ g^{-1}$, respectively. Pore size diameters were assessed using non-local density functional theory, revealing TPET-Bimine (1.01 and 2.06 nm), PT-Bimine (1.77 nm), TPET-Im (1.06 and 1.99 nm), and PT-Im (2.58 and 4.84 nm) CMPs. This suggests that TPET-Bimine, PT-Bimine, and TPET-Im CMPs exhibit micro/mesoporous characteristics, while PT-Im demonstrates microporous behavior. The surface morphologies of TPET-Bimine, PT-Bimine, TPET-Im, and PT-Im CMPs were observed through SEM [Fig. 4 (a–h)]. All CMPs exhibited amorphous surfaces and clustered shapes. High-resolution TEM provided further evidence of their microporous characteristics. HR-TEM images [Fig. 4(i–l)] revealed that both bimine-linked CMPs and Im-linked CMPs

Published on 27 December 2023. Downloaded by National Sun Yat Sen University on 5/13/2024 10:20:48 AM.

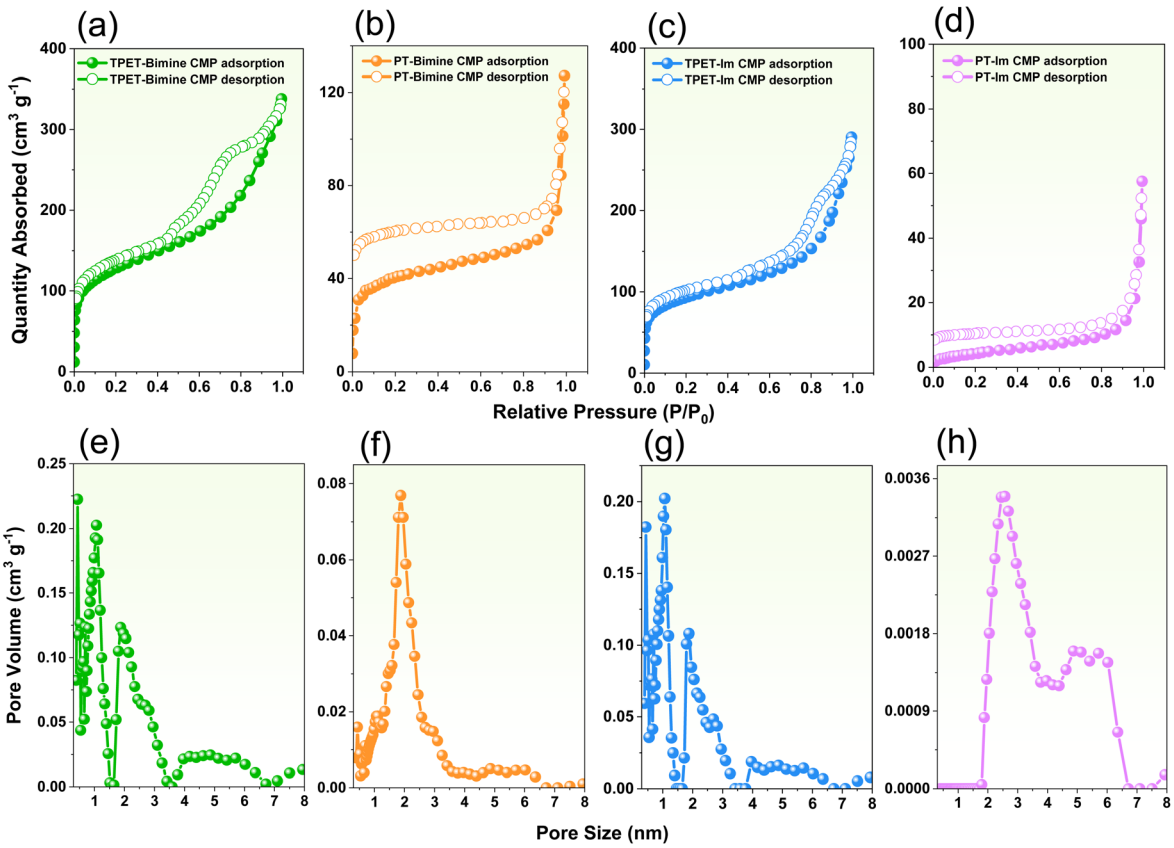

Fig. 3 BET (a–d) and pore diameter (e–h) profiles of TPET-Bimine CMP (a and e), PT-Bimine CMP (b and f), TPET-Im CMP (c and g) and PT-Im CMP (d and h).

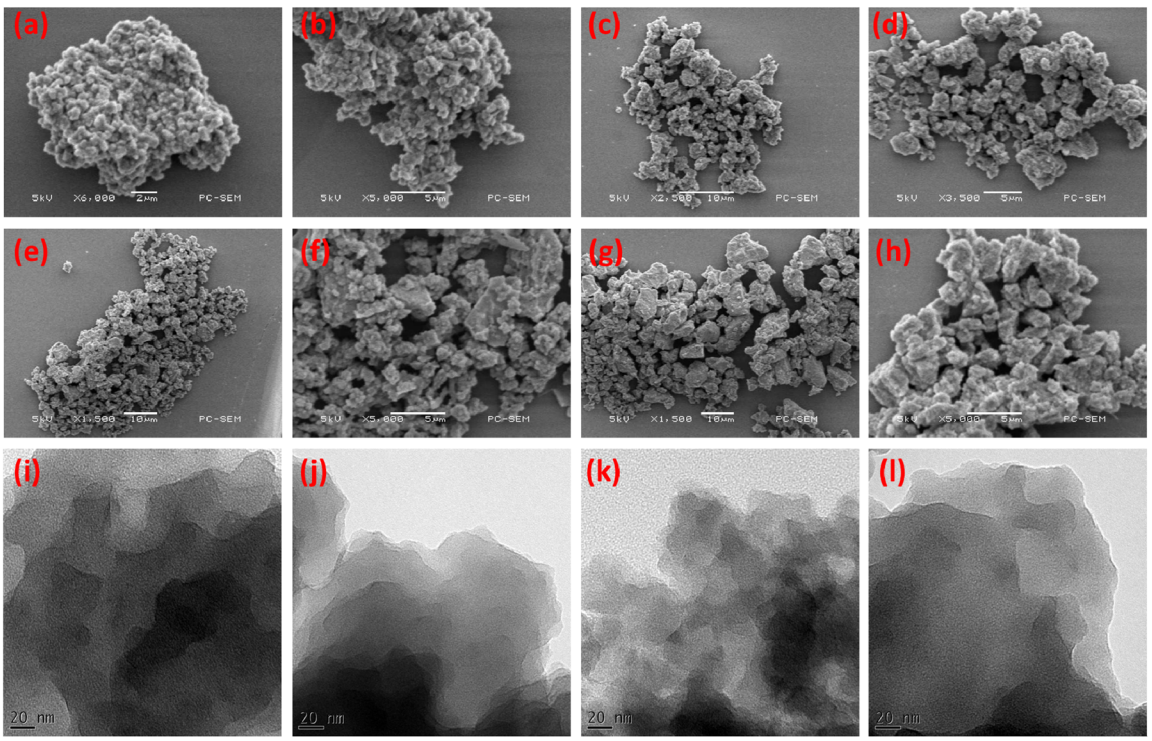

Fig. 4 SEM (a–h) and TEM (i–l) profiles of TPET-Bimine CMP (a, b and i), PT-Bimine CMP (c, d and j), TPET-Im CMP (e, f and k) and PT-Im CMP (g, h and l).

This journal is © The Royal Society of Chemistry 2024

Published on 27 December 2023. Downloaded by National Sun Yat Sen University on 5/13/2024 10:20:48 AM.

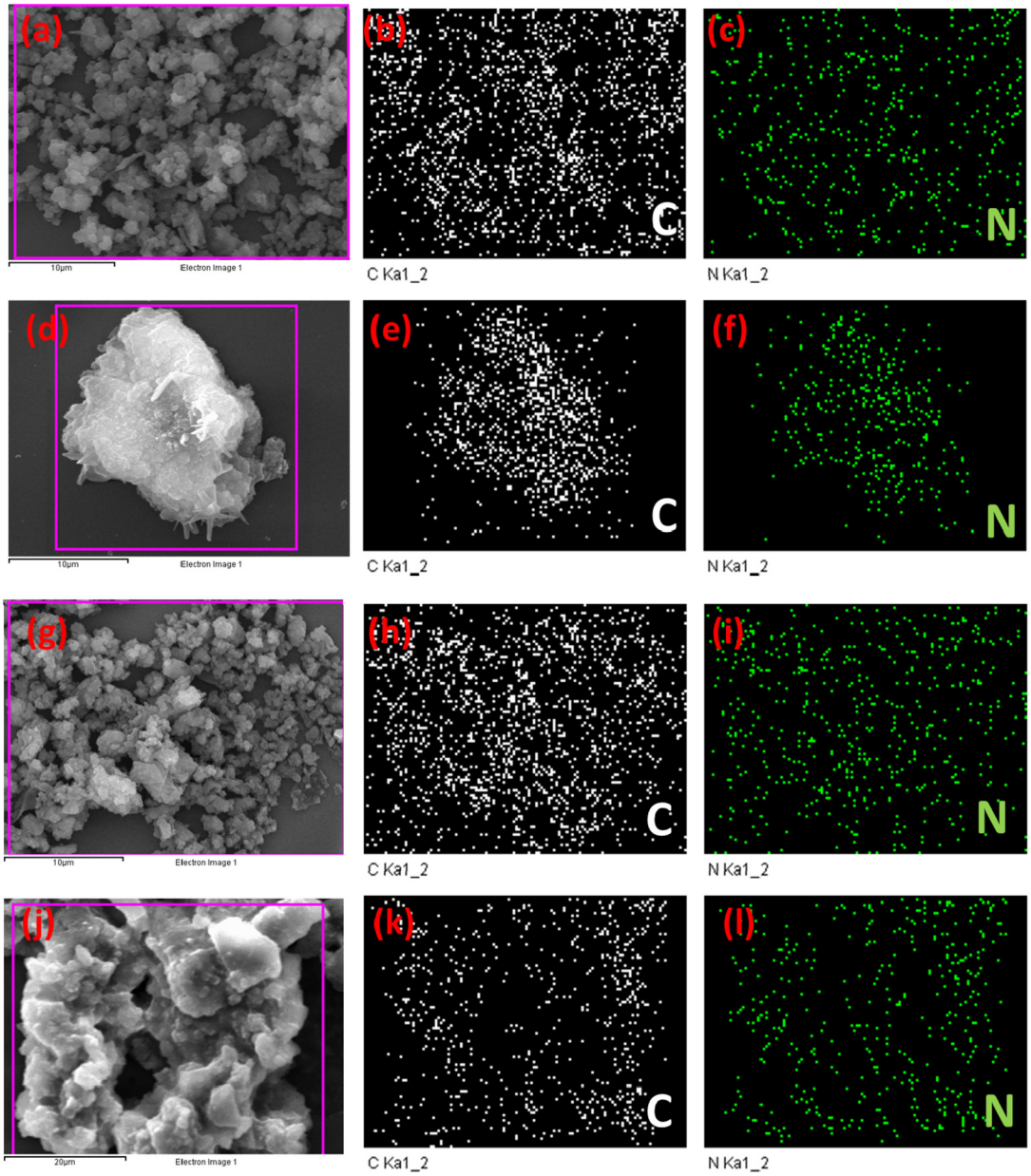

Fig. 5 SEM-EDS mapping of TPET-Bimine CMP (a–c), PT-Bimine CMP (d–f), TPET-Im CMP (g–i) and PT-Im CMP (j–l).

feature a porous network architecture. Elemental area mapping of bimine-linked CMPs and Im-linked CMPs using energy-dispersive X-ray spectroscopy (EDS) demonstrated a uniform distribution of C and N atoms within their frameworks, represented by the colors white and green, respectively, as shown in Fig. 5. Analysis using PXRD indicated that both TPET-Bimine and PT-Bimine CMPs possess an amorphous nature, as evidenced by the presence of broad peaks (Fig. S6†).

Antibacterial activities of bimine-linked CMPs and Im-linked CMPs

The study assessed the efficacy of different concentrations of PT-Bimine, PT-Im, TPET-Bimine, and TPET-Im CMPs against *S. aureus*. The microbial suspension was exposed to these CMPs for 18 hours, and solution droplets were subsequently placed on agar plates. The experimental results are summarized in Fig. 6(a). PT-Bimine and TPET-Bimine CMPs, lacking imidazolium modification, exhibited minimal antibacterial activity. In contrast, PT-Im and TPET-Im CMPs demonstrated robust antibacterial effects, primarily attributed to the presence of the imidazolium cation in imidazolium-linked CMPs, showcasing potent antibacterial properties. At a concentration of 15 mg mL^{-1}, the bactericidal activity of the PT-Im and TPET-Im CMPs was maximum. The imidazolium cation of these CMPs and the negatively charged microbial surface interact electrostatically to produce the antibacterial mechanism.

Published on 27 December 2023. Downloaded by National Sun Yat Sen University on 5/13/2024 10:20:48 AM.

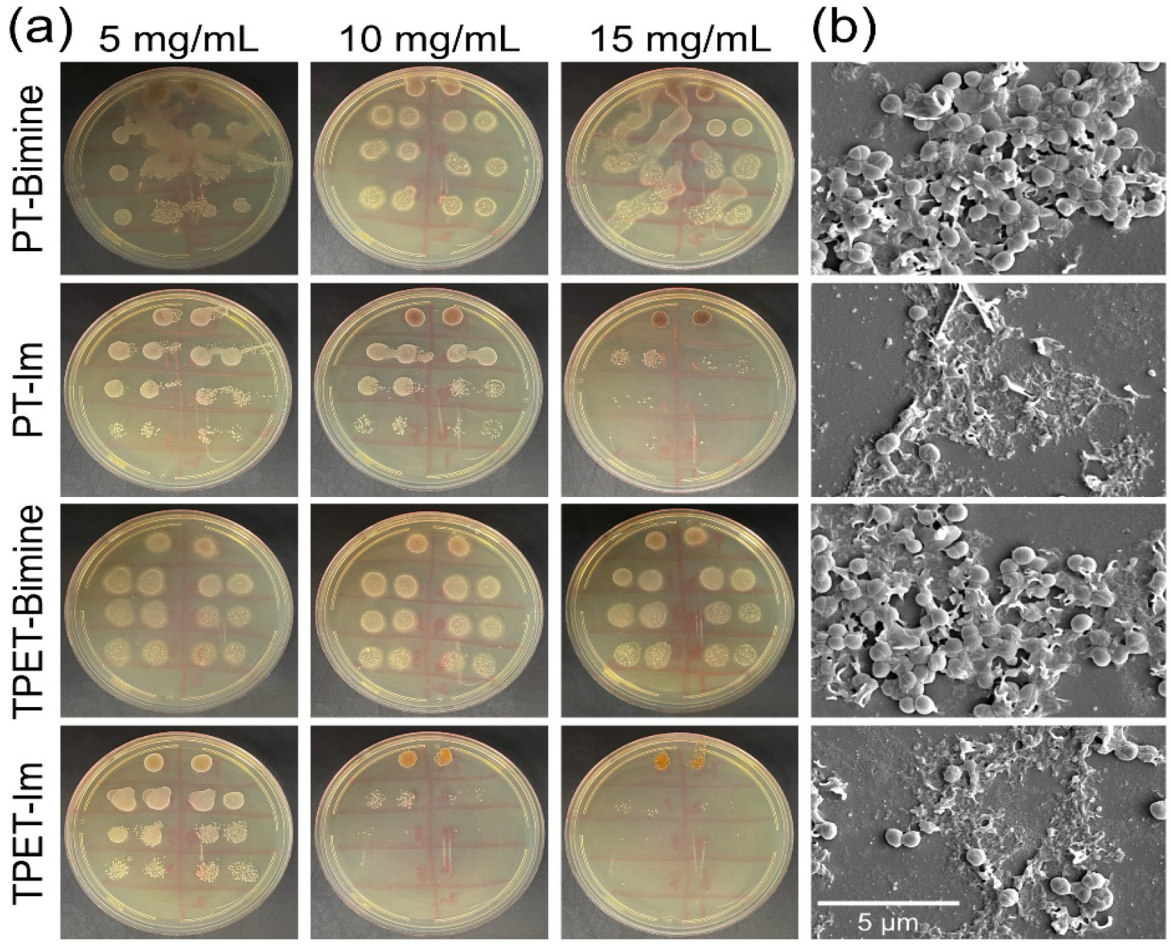

Fig. 6 Antibacterial activity of PT-Bimine, PT-Im, TPET-Bimine and TPET-Im CMPs against *S. aureus* (a) Agar plate image of *S. aureus* incubated for 18 h with CMPs at concentrations of 5, 10 and 15 mg mL^{-1} (b) SEM image of *S. aureus* incubated for 18 h with CMPs at a concentration of 15 mg mL^{-1}.

Electrostatic adsorption attracts the imidazolium cation to the anionic microbial cell wall. This interaction modifies the surface appearance of bacteria and increases the permeability of the cell wall by interacting with cations such as Mg^{2+} and Ca^{2+} within the cell wall. Furthermore, these CMPs' hydrophobic components can pierce the hydrophobic portion of the cell membrane, breaking microorganisms' cell membranes. The demise of microorganisms stems from an inability to maintain regular osmotic pressure when their cell membranes are disrupted. The potent antibacterial activity of PT-Im and TPET-Im CMPs is attributed to robust electrostatic interactions between the cationic CMPs and anionic microbial cell walls. Previous research suggests that Im-linked CMPs share a comparable antibacterial mechanism.[60]

This study employs SEM images to explore alterations in the microscopic morphology of bacteria following antibacterial treatment. Through the analysis of SEM images, this investigation explores alterations in the microscopic morphology of bacteria post-antibacterial treatment. Bacteria subjected to PT-Bimine and TPET-Bimine CMPs exhibited smooth, unblemished surfaces and formed clusters resembling grapes [Fig. 6(b)]. This distinctive characteristic corresponds to the biological activities of the *S. aureus* cell wall. Conversely, *S. aureus* treated with PT-Im and TPET-Im CMPs displayed a rugged, uneven surface morphology, indicating significant damage to the cell membrane [Fig. 6(b)]. This observation suggests that the cell membrane structure of *S. aureus* was penetrated and collapsed, rendering the distorted *S. aureus* biologically inactive following treatment with PT-Im and TPET-Im CMPs. The SEM images provided offer additional evidence of the robust antibacterial activity exhibited by our novel synthetic Im-linked CMPs.

The cytocompatibility of bimine-linked CMPs and Im-linked CMPs

Assessing cytotoxicity is crucial for materials intended for antibacterial applications, necessitating low toxicity to human cells. In this study, the cytotoxicity of CMPs was evaluated using a standard MTT assay. As shown in Fig. 7(a), PT-Bimine, PT-Im, TPET-Bimine, and TPET-Im CMPs exhibited cell viability values of 112.1%, 112.5%, 120.3%, and 104.7%, respectively. These results indicate that at a concentration of 5 mg

 This journal is © The Royal Society of Chemistry 2024

Published on 27 December 2023. Downloaded by National Sun Yat Sen University on 5/13/2024 10:20:48 AM.

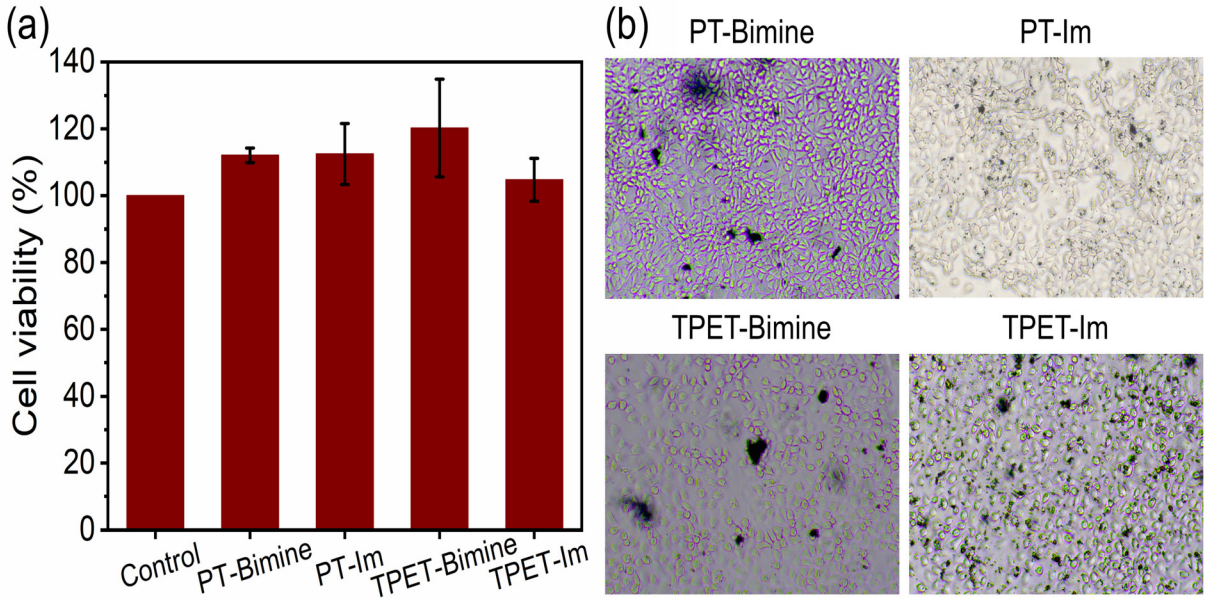

Fig. 7 (a) MTT assessment of the cytotoxicity of PT-Bimine, PT-Im, TPET-Bimine, and TPET-Im CMPs against L929 fibroblasts. (b) Optical microscope images of L929 fibroblasts cultured for 48 hours using a concentration of 5 mg mL^{-1} of CMPs. The MTT results and corresponding error bars are the standard deviation values from three independent experiments.

mL^{-1}, the CMPs had no toxic effects on L929 fibroblasts. Furthermore, the optical microscope images [Fig. 7(b)] revealed the typical proliferation and spreading morphology of L929 fibroblasts, demonstrating excellent cytocompatibility across all groups, aligning with the outcomes of the cell viability assay. These findings highlight the excellent biocompatibility of our novel CMPs, suggesting them as a cost-effective and safe alternative to hazardous and expensive chemicals for antibacterial applications. This positions them with promising potential as antibacterial materials.

Electrochemical performance of the bimine-linked CMPs and Im-linked CMPs

The prepared conductive bimine-linked CMPs and Im-linked CMPs underwent cyclic voltammetry (CV) and galvanostatic charge–discharge (GCD) tests to evaluate their electrochemical performance as potential electrode materials for energy storage applications. Working, reference, and counter electrodes were made of glassy carbon, mercury, and platinum, respectively, immersed in a 1.0 M KOH aqueous electrolyte, with a potential range of 0 to −1.0 V. CV curves [Fig. 8(a–d)] were obtained for TPET-Bimine CMP, PT-Bimine CMP, TPET-Im CMP, and PT-Im CMP at various scan speeds (5 to 200 mV s^{-1}). These compounds consistently exhibited a distinctive humped structure resembling a rectangle, indicating stability during current sweeps and accurate representation of capacitance from EDLC. The compounds demonstrated simple kinetics and high-rate capacity, as evidenced by the CV curves.[61–63] The CV profiles [Fig. 8] of both Bimine and Im-linked CMPs exhibit distinct humps, implying potential pseudocapacitance responses. These observable humps are ascribed to the existence of electron-rich phenyl groups and nitrogen, indicating their likely impact on the electrochemical characteristics of these compounds, and the mechanism is shown in Fig. S7.†[64,65] Capacitance and GCD profiles [Fig. 8(e–h)] were further explored at current densities ranging from 0.5 A g^{-1} to 20 A g^{-1}. The bent-triangular shape of the (GCD) curves pointed towards the EDLC and pseudocapacitive characteristics of the compounds. Specific capacitance measurements [Fig. 9(a)] at different current densities (5, 10, 20, 30, 50, 70, 100, and 200 A g^{-1}) revealed varying performance levels. For instance, PT-Im CMP exhibited specific capacitances of 53, 20, 9, 7, 6, 5, 4.8, 4.6, and 4.2 F g^{-1}, while PT-Bimine CMP delivered 37, 20, 16, 12, 10, 9, 8, 7.6, and 7 F g^{-1}. In comparison, TPET-Im CMP showed specific capacitances of 63, 27, 17, 15, 12, 11, 10, 9.5, and 9.4 F g^{-1}, and TPET-Bimine CMP exhibited 34, 17, 13, 11, 10, 9.8, 9.2, 8.5, and 8 F g^{-1}. The specific capacitance trends followed the order: TPET-Im CMP > PT-Im CMP > PT-Bimine CMP > TPET-Bimine CMP. These trends suggest the superior performance of imidazolium-based compounds over bimine-based ones, emphasizing the potential of Imidazolium in enhancing capacitance in these energy storage applications. Moreover, TPET-Im CMP, PT-Im CMP, PT-Bimine CMP, and TPET-Bimine CMP achieved energy densities of 8.73, 7.36, 5.14, and 4.75 W h kg^{-1}, respectively [Fig. 9(b)]. As depicted in the stability plots [Fig. 10(a)], both Im-linked CMPs (specifically TPET-Im and PT-Im CMPs) exhibited superior durability properties compared to their bimine-linked CMPs precursors. The enhanced specific retention observed in Im-CMPs compared to their bimine-linked counterparts could be attributed to the incorporation of an imidazolium (Im) ring in the Im-CMPs framework. The capacity values for TPET-Im CMP and

Published on 27 December 2023. Downloaded by National Sun Yat Sen University on 5/13/2024 10:20:48 AM.

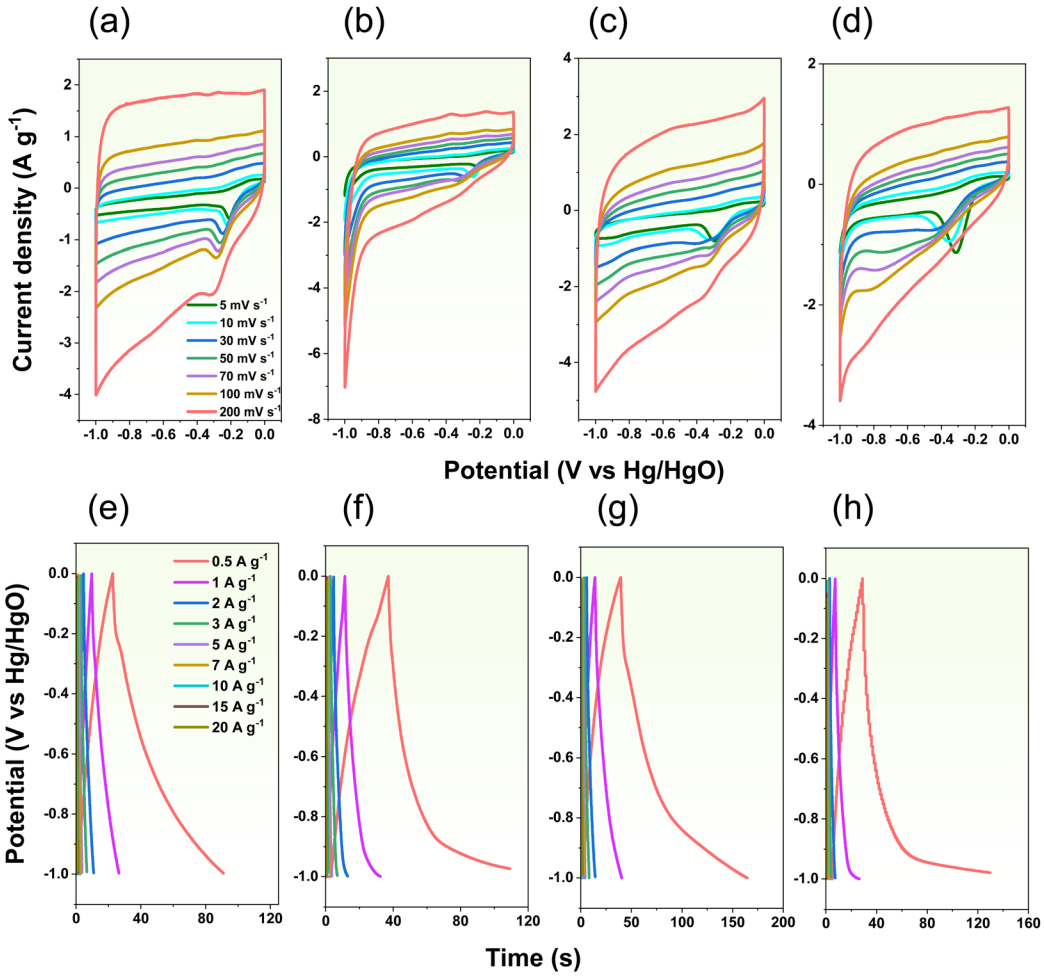

Fig. 8 CV (a–d) and GCD (e–h) profiles of TPET-Bimine CMP (a and e), PT-Bimine CMP (b and f), TPET-Im CMP (c and g) and PT-Im CMP (d and h).

PT-Im CMP surpassed those of other porous candidate materials for SCs applications, as illustrated in Fig. 10(b) and Table S1.†

The Electrochemical Impedance Spectroscopy (EIS) was used to analyze Bimine and Im linked CMPs. Nyquist spectra are depicted in Fig. S8(a) and S8(b).† Notably, the lines for TPET-Bimine and TPET-Im CMP cells are shorter than those of the other cells, with the TPET-Bimine CMP line leaning towards the vertical Z'' axis, suggesting superior capacitance performance.[65–72] The straight lines departing from the vertical axis indicate that none of the other cells have a greater Warburg length or resistance compared to TPET-Bimine CMP. The ohmic resistances of PT-Im CMP, PT-Bimine CMP, TPET-Im CMP, and TPET-Bimine CMP were measured at 1.68, 0.75, 0.93, and 0.51 Ω, respectively. The frequency-dependent magnitude Bode plot, presented in Fig. S8(c),† supports the exceptional capacitive properties of the electrode materials. Slant lines with a negative slope at low frequencies and negligible resistance at high frequencies confirm the superior capacitive behavior. Fig. S8(d)† also illustrates phase angle plots varying with frequency for the electrodes. The knee frequencies, where the phase angle reaches −45° indicating equal capacitive and resistive characteristics were identified. Notably, PT-Bimine and PT-Im CMP exhibit knee frequencies of 1599.43 and 711.12 Hz, respectively, while TPET-Bimine and TPET-Im CMPs show comparable knee frequencies of 437.57 Hz. These knee frequency values are indicative of the rate capability of the compounds and their proportional connection, further validating their outstanding electrochemical performance. To investigate the practical applications of TPET-Bimine CMP, PT-Bimine CMP, TPET-Im CMP, and PT-Im CMP, we assembled two-electrode symmetric coin cell devices, as illustrated in Fig. S9.† The CV curves were examined across various scan speeds ranging from 5 mV s^{-1} to 200 mV s^{-1} within the potential window of 0 to +0.5 V. Notably, these CMP materials displayed quasitriangular forms with discernible humps, indicating a combination of electric double-layer capacitance (EDLC) and pseudocapacitance behavior, as depicted in Fig. S9 (a–d).† Importantly, the CV curves for TPET-Bimine CMP, PT-Bimine CMP, TPET-Im CMP, and PT-Im CMP devices maintain a stable and acceptable form even as the scanning rate progressively increases. As the current density rises,

 This journal is © The Royal Society of Chemistry 2024

Published on 27 December 2023. Downloaded by National Sun Yat Sen University on 5/13/2024 10:20:48 AM.

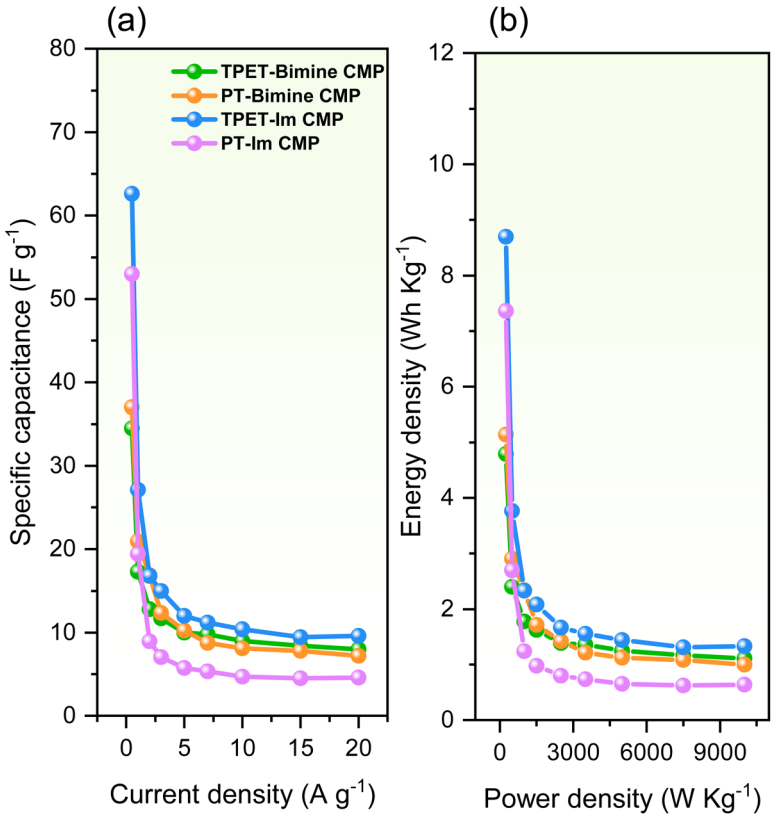

Fig. 9 (a) Specific capacitance and (b) Ragone profile of TPET-Bimine CMP, PT-Bimine CMP, TPET-Im CMP and PT-Im CMP.

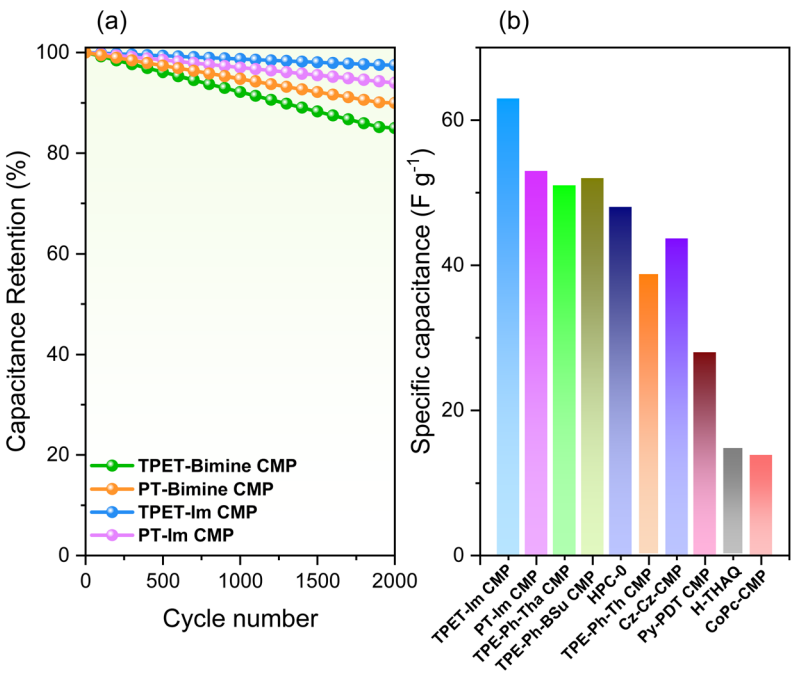

Fig. 10 (a) Specific retention pattern of TPET-Bimine CMP, PT-Bimine CMP, TPET-Im CMP and PT-Im CMP and (b) comparing the specific capacitance profiles of TPET-Im CMP and PT-Im CMP to those of other previously reported materials.

Published on 27 December 2023. Downloaded by National Sun Yat Sen University on 5/13/2024 10:20:48 AM.

Fig. S9(e–h)† depict the GCD curves for TPET-Bimine CMP, PT-Bimine CMP, TPET-Im CMP, and PT-Im CMP. It is observable that with the escalating current density, the discharging time of the electrode material diminishes, leading to a proportional decrease in specific capacitance. Notably, the highest specific capacitance is observed at 0.5 A g^{-1}, as illustrated in Fig. S10(a).† At a current density of 0.5 A g^{-1}, the determined specific capacitances for TPET-Bimine CMP, PT-Bimine CMP, TPET-Im CMP, and PT-Im CMP were 23.35, 31.6, 37.26, and 35 F g^{-1}, respectively [Fig. S9(a)†]. Moreover, as depicted in Fig. S10(b),† the achieved energy densities for TPET-Bimine CMP, PT-Bimine CMP, TPET-Im CMP, and PT-Im CMP were 3.24, 4.39, 5.18, and 4.86 W h kg^{-1}, respectively.

Conclusions

In summary, we successfully synthesized bimine-linked CMPs and subjected them to a post-modification process, transforming them into imidazolium (Im)-included CMPs. These modified CMPs were then evaluated for their dual functionality as antibacterial agents and supercapacitor electrode materials. The incorporation of the imidazolium moiety not only enhanced antibacterial properties but also improved electrochemical performance. The cationic charges facilitated robust interactions with bacterial membranes, thereby elevating antibacterial efficacy, particularly against *S. aureus*. The antibacterial study revealed a concentration-dependent increase in activity, with PT-Im and TPET-Im CMPs exhibiting the highest antibacterial efficacy at a concentration of 15 mg mL^{-1}. Furthermore, we assessed the cytocompatibility of all CMPs by examining their cytotoxicity against L929 fibroblasts, demonstrating excellent extrinsic cytocompatibility. Electrochemical evaluations indicated remarkable capacitance for TPET-Im and PT-Im CMPs, reaching 63 and 53 F g^{-1}, respectively, at a current density of 0.5 A g^{-1}. Due to their tunable structure, facile production, superior antibacterial activity, minimal toxicity, favorable porosity, good capacitance, and robust physicochemical stability, our Im-linked CMPs exhibit promising potential for diverse applications, including antibacterial treatments and energy storage.

Author contributions

Aya Osama Mousa: investigation, methodology, writing – original draft. Zheng-Ian Lin: investigation. Swetha V Chaganti: investigation. Cheng-Hsin Chuang: supervision. Chih-Kuang Chen: supervision. Shiao-Wei Kuo: supervision. Mohamed Gamal Mohamed: investigation: methodology, conceptualization, supervision, writing – original draft.

Conflicts of interest

There are no conflicts to declare.

Acknowledgements

This study was supported financially by the Ministry of Science and Technology, Taiwan, under contracts NSTC 112-2218-E-110-007 and 112-2223-E-110-002. The authors thank the staff at National Sun Yat-sen University for their assistance with the TEM (ID: EM022600) experiments.

References

1 K. C. Nicolaou and S. Rigol, A brief history of antibiotics and select advances in their synthesis, *J. Antibiot.*, 2018, **71**, 153–184.
2 G. Muteeb, M. T. Rehman, M. Shahwan and M. Aatif, Origin of Antibiotics and Antibiotic Resistance, and Their Impacts on Drug Development: A Narrative Review, *Pharmaceuticals*, 2023, **16**, 1615.
3 C. Bathula, M. K. Ravindra, A. Kumar, H. Yadav, S. Ramesh, S. Shinde, N. K. Shrestha, K. M. Mahadevan, V. Reddy and A. Mohammed, Microwave assisted synthesis of imidazolyl fluorescent dyes as antimicrobial agents, *J. Mater. Res. Technol.*, 2020, **9**, 6900–6908.
4 E. M. Darby, E. Trampari, P. Siasat, M. S. Gaya, I. Alav, M. A. Webber and J. M. Blair, Molecular mechanisms of antibiotic resistance revisited, *Nat. Rev. Microbiol.*, 2023, **21**, 280–295.
5 D. Pranantyo, K. Zhang, Z. Si, Z. Hou and M. B. Chan-Park, Smart multifunctional polymer systems as alternatives or supplements of antibiotics to overcome bacterial resistance, *Biomacromolecules*, 2022, **23**, 1873–1891.
6 D. Nwobodo, M. C. Ugwu, C. O. Anie, M. T. S. Al-Ouqaili, J. C. Ikem, U. V. Chigozie and M. Saki, Antibiotic resistance: The challenges and some emerging strategies for tackling a global menace, *J. Clin. Lab. Anal.*, 2022, **36**, e24655.
7 P. R. Judzewitsch, T. K. Nguyen, S. Shanmugam, E. H. Wong and C. Boyer, Towards sequence–controlled antimicrobial polymers: effect of polymer block order on antimicrobial activity, *Angew. Chem., Int. Ed.*, 2018, **57**, 4559–4564.
8 R. Namivandi-Zangeneh, R. J. Kwan, T.-K. Nguyen, J. Yeow, F. L. Byrne, S. H. Oehlers, E. H. Wong and C. Boyer, Correction: The effects of polymer topology and chain length on the antimicrobial activity and hemocompatibility of amphiphilic ternary copolymers, *Polym. Chem.*, 2018, **9**, 1745–1745.
9 J. Zhang, Y. P. Chen, K. P. Miller, M. S. Ganewatta, M. Bam, Y. Yan, M. Nagarkatti, A. W. Decho and C. Tang, Antimicrobial metallopolymers and their bioconjugates with conventional antibiotics against multidrug-resistant bacteria, *J. Am. Chem. Soc.*, 2014, **136**, 4873–4876.
10 P. Li, Y. F. Poon, W. Li, H.-Y. Zhu, S. H. Yeap, Y. Cao, X. Qi, C. Zhou, M. Lamrani and R. W. Beuerman, A polycationic antimicrobial and biocompatible hydrogel with microbe

 This journal is © The Royal Society of Chemistry 2024

Published on 27 December 2023. Downloaded by National Sun Yat Sen University on 5/13/2024 10:20:48 AM.

membrane suctioning ability, *Nat. Mater.*, 2011, **10**, 149–156.

11 W. Ji, R. R. Koepsel, H. Murata, S. Zadan, A. S. Campbell and A. J. Russell, Bactericidal specificity and resistance profile of poly (quaternary ammonium) polymers and protein–poly (quaternary ammonium) conjugates, *Biomacromolecules*, 2017, **18**, 2583–2593.

12 L. Liu, K. Xu, H. Wang, P. J. Tan, W. Fan, S. S. Venkatraman, L. Li and Y.-Y. Yang, Self-assembled cationic peptide nanoparticles as an efficient antimicrobial agent, *Nat. Nanotechnol.*, 2009, **4**, 457–463.

13 G. N. Tew, R. W. Scott, M. L. Klein and W. F. DeGrado, De novo design of antimicrobial polymers, foldamers, and small molecules: from discovery to practical applications, *Acc. Chem. Res.*, 2010, **43**, 30–39.

14 N. Wiradharma, U. Khoe, C. A. Hauser, S. V. Seow, S. Zhang and Y.-Y. Yang, Synthetic cationic amphiphilic α-helical peptides as antimicrobial agents, *Biomaterials*, 2011, **32**, 2204–2212.

15 A. Mollahosseini, A. Rahimpour, M. Jahamshahi, M. Peyravi and M. Khavarpour, The effect of silver nanoparticle size on performance and antibacteriality of polysulfone ultrafiltration membrane, *Desalination*, 2012, **306**, 41–50.

16 Y. Orooji, M. Ghanbari, O. Amiri and M. Salavati-Niasari, Facile fabrication of silver iodide/graphitic carbon nitride nanocomposites by notable photo-catalytic performance through sunlight and antimicrobial activity, *J. Hazard. Mater.*, 2020, **389**, 122079.

17 S. Venkataraman, Y. Zhang, L. Liu and Y.-Y. Yang, Design, syntheses and evaluation of hemocompatible pegylated-antimicrobial polymers with well-controlled molecular structures, *Biomaterials*, 2010, **31**, 1751–1756.

18 Z. Song, Z. Han, S. Lv, C. Chen, L. Chen, L. Yin and J. Cheng, Synthetic polypeptides: from polymer design to supramolecular assembly and biomedical application, *Chem. Soc. Rev.*, 2017, **46**, 6570–6599.

19 P.-Y. Wang, H.-S. Fang, W.-B. Shao, J. Zhou, Z. Chen, B.-A. Song and S. Yang, Synthesis and biological evaluation of pyridinium-functionalized carbazole derivatives as promising antibacterial agents, *Bioorg. Med. Chem. Lett.*, 2017, **27**, 4294–4297.

20 J. Qin, J. Guo, Q. Xu, Z. Zheng, H. Mao and F. Yan, Synthesis of pyrrolidinium-type poly (ionic liquid) membranes for antibacterial applications, *ACS Appl. Mater. Interfaces*, 2017, **9**, 10504–10511.

21 N. Beyth, I. Yudovin-Farber, R. Bahir, A. J. Domb and E. I. Weiss, Antibacterial activity of dental composites containing quaternary ammonium polyethylenimine nanoparticles against Streptococcus mutans, *Biomaterials*, 2006, **27**, 3995–4002.

22 N. Iwai, K. Nakayama and T. Kitazume, Antibacterial activities of imidazolium, pyrrolidinium and piperidinium salts, *Bioorg. Med. Chem. Lett.*, 2011, **21**, 1728–1730.

23 Z. Zheng, Q. Xu, J. Guo, J. Qin, H. Mao, B. Wang and F. Yan, Structure–antibacterial activity relationships of imidazolium-type ionic liquid monomers, poly (ionic liquids) and poly (ionic liquid) membranes: effect of alkyl chain length and cations, *ACS Appl. Mater. Interfaces*, 2016, **8**, 12684–12692.

24 S. N. Riduan and Y. Zhang, Imidazolium salts and their polymeric materials for biological applications, *Chem. Soc. Rev.*, 2013, **42**, 9055–9070.

25 J. Guo, J. Qin, Y. Ren, B. Wang, H. Cui, Y. Ding, H. Mao and F. Yan, Antibacterial activity of cationic polymers: side-chain or main-chain type?, *Polym. Chem.*, 2018, **9**, 4611–4616.

26 A. O. Mousa, M. G. Mohamed, C.-H. Chuang and S.-W. Kuo, Carbonized Aminal-Linked Porous Organic Polymers Containing Pyrene and Triazine Units for Gas Uptake and Energy Storage, *Polymers*, 2023, **15**, 1891.

27 M. G. Mohamed, H.-Y. Hu, M. Madhu, M. M. Samy, I. M. Mekhemer, W.-L. Tseng, H.-H. Chou and S.-W. Kuo, Ultrastable Two-Dimensional Fluorescent Conjugated Microporous Polymers Containing Pyrene and Fluorene Units for Metal Ion Sensing and Energy Storage, *Eur. Polym. J.*, 2023, 111980.

28 M. G. Mohamed, W.-C. Chang, S. V. Chaganti, S. U. Sharma, J.-T. Lee and S.-W. Kuo, Dispersion of ultrastable crown-ether-functionalized triphenylamine and pyrene-linked porous organic conjugated polymers with single-walled carbon nanotubes as high-performance electrodes for supercapacitors, *Polym. Chem.*, 2023, **14**, 4589–4601.

29 M. M. Samy, M. G. Mohamed and S.-W. Kuo, Conjugated Microporous Polymers Based on Ferrocene Units as Highly Efficient Electrodes for Energy Storage, *Polymers*, 2023, **15**, 1095.

30 A. O. Mousa, C.-H. Chuang, S.-W. Kuo and M. G. Mohamed, Strategic Design and Synthesis of Ferrocene Linked Porous Organic Frameworks toward Tunable CO_2 Capture and Energy Storage, *Int. J. Mol. Sci.*, 2023, **24**, 12371.

31 M. G. Mohamed, S.-Y. Chang, M. Ejaz, M. M. Samy, A. O. Mousa and S.-W. Kuo, Design and Synthesis of Bisulfone-Linked Two-Dimensional Conjugated Microporous Polymers for CO_2 adsorption and Energy Storage, *Molecules*, 2023, **28**, 3234.

32 M. Ejaz, M. G. Mohamed, W.-C. Huang and S.-W. Kuo, Pyrene-based covalent organic polymers with nano carbonaceous composites for efficient supercapacitive energy storage, *J. Mater. Chem. A*, 2023, **11**, 22868–22883.

33 C.-Y. Chen, M. G. Mohamed, W. C. Chen and S.-W. Kuo, Construction of Ultrastable porous carbons materials derived from organic/inorganic double-decker silsesquioxane (DDSQ) hybrid as a high-performance electrode for supercapacitor, *Mater. Today Chem.*, 2023, **34**, 101773.

34 P. N. Singh, M. G. Mohamed, S. V. Chaganti, S. U. Sharma, M. Ejaz, J.-T. Lee and S.-W. Kuo, Rational Design of Ultrastable Conjugated Microporous Polymers Based on Pyrene and Perylene Units as High-Performance Organic

Published on 27 December 2023. Downloaded by National Sun Yat Sen University on 5/13/2024 10:20:48 AM.

Electrode Materials for Supercapacitor Applications, *ACS Appl. Energy Mater.*, 2023, **6**, 8277–8287.

35 S. A. Patil, P. K. Katkar, M. Kaseem, G. Nazir, S. W. Lee, H. Patil, H. Kim, V. K. Magotra, H. B. Thi, H. Im and N. K. Shrestha, Cu@Fe-Redox Capacitive-Based Metal–Organic Framework Film for a High-Performance Supercapacitor Electrode, *Nanomaterials*, 2023, **13**, 1587.

36 R. B. Ambade, S. B. Ambade, N. K. Shrestha, R. R. Salunkhe, W. Lee, S. S. Bagde, J. H. Kim, F. J. Stadler, Y. Yamauchi and S. H. Lee, Controlled growth of polythiophene nanofibers in TiO_2 nanotube arrays for supercapacitor applications, *J. Mater. Chem. A*, 2017, **5**, 172–180.

37 M. G. Mohamed, H.-Y. Hu, S. Santhoshkumar, M. Madhu, T. H. Mansoure, C.-W. Hsiao, Y. Ye, C.-W. Huang, W.-L. Tseng and S.-W. Kuo, Design and Synthesis of Bifunctional Conjugated Microporous Polymers Containing Tetraphenylethene and Bisulfone Units for Energy Storage and Fluorescent Sensing of p-Nitrophenol, *Colloids Surf., A*, 2024, **680**, 132675.

38 D. Y. Lee, S. J. Yoon, N. K. Shrestha, S. H. Lee, H. Ahn and S. H. Han, Unusual energy storage and charge retention in Co-based metal–organic-frameworks, *Microporous Mesoporous Mater.*, 2012, **153**, 163–165.

39 D. Y. Lee, D. V. Shinde, E. K. Kim, W. Lee, I. W. Oh, N. K. Shrestha, J. K. Lee and S. H. Han, Supercapacitive property of metal–organic-frameworks with different pore dimensions and morphology, *Microporous Mesoporous Mater.*, 2013, **171**, 53–57.

40 M. M. Samy, M. G. Mohamed, S. U. Sharma, S. V. Chaganti, T. H. Mansoure, J.-T. Lee, T. Chen and S.-W. Kuo, Constructing conjugated microporous polymers containing triphenylamine moieties for high-performance capacitive energy storage, *Polymer*, 2023, **264**, 125541.

41 M. G. Mohamed, A. F. El-Mahdy, M. G. Kotp and S.-W. Kuo, Advances in porous organic polymers: Syntheses, structures, and diverse applications, *Mater. Adv.*, 2022, **3**, 707–733.

42 M. G. Mohamed, M. H. Elsayed, A. M. Elewa, A. F. M. El-Mahdy, C.-H. Yang, A. A. Mohammed, H.-H. Chou and S.-W. Kuo, Pyrene-containing conjugated organic microporous polymers for photocatalytic hydrogen evolution from water, *Catal. Sci. Technol.*, 2021, **11**, 2229–2241.

43 M. G. Mohamed, T. H. Mansoure, M. M. Samy, Y. Takashi, A. A. Mohammed, T. Ahamad, S. M. Alshehri, J. Kim, B. M. Matsagar and K. C.-W. Wu, Ultrastable Conjugated Microporous Polymers Containing Benzobisthiadiazole and Pyrene Building Blocks for Energy Storage Applications, *Molecules*, 2022, **27**, 2025.

44 M. G. Mohamed, T.-C. Chen and S.-W. Kuo, Solid-state chemical transformations to enhance gas capture in benzoxazine-linked conjugated microporous polymers, *Macromolecules*, 2021, **54**, 5866–5877.

45 T.-H. Weng, M. G. Mohamed, S. U. Sharma, S. V. Chaganti, M. M. Samy, J.-T. Lee and S.-W. Kuo, Ultrastable three-dimensional triptycene-and tetraphenylethene-conjugated microporous polymers for energy storage, *ACS Appl. Energy Mater.*, 2022, **5**, 14239–14249.

46 Y. Zhu, P. Xu, X. Zhang and D. Wu, Emerging porous organic polymers for biomedical applications, *Chem. Soc. Rev.*, 2022, **51**, 1377–1414.

47 P. Palani and S. Karpagam, Conjugated polymers–a versatile platform for various photophysical, electrochemical and biomedical applications: a comprehensive review, *New J. Chem.*, 2021, **45**, 19182–19209.

48 Y. Wang, Q. Yuan, M. Li and Y. Tang, Cationic Conjugated Microporous Polymers Coating for Dual–Modal Antimicrobial Inactivation with Self–Sterilization and Reusability Functions, *Adv. Funct. Mater.*, 2023, 2213440.

49 C. W. Hsiao, A. M. Elewa, M. G. Mohamed and S. W. Kuo, Highly stable hybrid porous polymers containing polyhedral oligomeric silsesquioxane (POSS)/Dibenzo[g,p]chrysene and Dibenzo[b,d]thiophene units for efficient Rhodamine B dye removal, *Sep. Purif. Technol.*, 2024, **332**, 125771.

50 A. O. Mousa, M. G. Mohamed, Z.-I. Lin, C.-H. Chuang, C.-K. Chen and S.-W. Kuo, Conjugated microporous polymers as a novel generation of drug carriers: A systemic study toward efficient carriers of tetracycline antibiotic, *Eur. Polym. J.*, 2023, **196**, 112254.

51 R. Gao, W. Zhao, Q. Qiu, A. Xie, S. Cheng, Y. Jiao, X. Pan and W. Dong, Fluorescent conjugated microporous polymer (CMP) derived sensor array for multiple Organic/Inorganic contaminants detection, *Sens. Actuators, B*, 2020, **320**, 128448.

52 F. Wang, F. Ren, D. Ma, P. Mu, H. Wei, C. Xiao, Z. Zhu, H. Sun, W. Liang and J. Chen, Particle and nanofiber shaped conjugated microporous polymers bearing hydantoin-substitution with high antibacterial activity for water cleanness, *J. Mater. Chem. A*, 2018, **6**, 266–274.

53 Y. Lei, Z. Zhu, H. Sun, P. Mu, W. Liang and A. Li, Conjugated microporous polymers bearing isocyanurate moiety as efficient antibacterial membrane and aerogels, *Sep. Purif. Technol.*, 2020, **248**, 117020.

54 M. Wu, Y. Han, B. Wang, Y. Yuan, C. Xing and Y. Chen, S, N-heteroacene-based conjugated microporous polymers as fluorescent sensors and effective antimicrobial carriers, *ACS Appl. Bio Mater.*, 2018, **1**, 473–479.

55 A. O. Mousa, Z.-I. Lin, C.-H. Chuang, C.-K. Chen, S.-W. Kuo and M. G. Mohamed, Rational Design of Bifunctional Microporous Organic Polymers Containing Anthracene and Triphenylamine Units for Energy Storage and Biological Applications, *Int. J. Mol. Sci.*, 2023, **24**, 8966.

56 T.-H. Weng, M. G. Mohamed, S. U. Sharma, I. M. Mekhemer, H.-H. Chou and S.-W. Kuo, Rationally Engineered Ultrastable Three-Dimensional (3D) Conjugated Microporous Polymers Containing Triptycene, Tetraphenylethene, and Benzothiadiazole Units as Exceptional High-Performance Organic Electrodes for Supercapacitors, *ACS Appl. Energy Mater.*, 2023, **6**, 9012–902457.

 This journal is © The Royal Society of Chemistry 2024

Published on 27 December 2023. Downloaded by National Sun Yat Sen University on 5/13/2024 10:20:48 AM.

57 M. G. Mohamed, C. C. Chen, K. Zhang and S. W. Kuo, Construction of three-dimensional porous organic polymers with enhanced CO_2 uptake performance via solid-state thermal conversion from tetrahedral benzoxazine-linked precursor, *Eur. Polym. J.*, 2023, **200**, 112551.

58 P. N. Singh, M. G. Mohamed and S. W. Kuo, Systematic Design and Synthesis of Conjugated Microporous Polymers Containing Pyrene and Azobenzene Building Materials for High-Performance Energy Storage, *ACS Appl. Energy Mater.*, 2023, **6**(21), 11342–11351.

59 M. G. Mohamed, W. C. Chang and S. W. Kuo, Crown Ether- and Benzoxazine-Linked Porous Organic Polymers Displaying Enhanced Metal Ion and CO_2 Capture through Solid-State Chemical Transformation, *Macromolecules*, 2022, **55**, 7879–7892, DOI: **10.1021/acs.macromol.2c01216**.

60 E. H. Mattar, H. A. Almehdar, H. A. Yacoub, V. N. Uversky and E. M. Redwan, Antimicrobial potentials and structural disorder of human and animal defensins, *Cytokine Growth Factor Rev.*, 2016, **28**, 95–111.

61 M. G. Mohamed, S. V. Chaganti, S. U. Sharma, M. M. Samy, M. Ejaz, J. T. Lee, K. Zhang and S. W. Kuo, Constructing Conjugated Microporous Polymers Containing the Pyrene-4,5,9,10-Tetraone Unit for Energy Storage, *ACS Appl. Energy Mater.*, 2022, **5**, 10130–10140.

62 M. G. Mohamed, M. M. Samy, T. H. Mansoure, S. U. Sharma, M. S. Tsai, J. H. Chen, J. T. Lee and S. W. Kuo, Dispersions of 1,3,4-Oxadiazole-Linked Conjugated Microporous Polymers with Carbon Nanotubes as a High-Performance Electrode for Supercapacitors, *ACS Appl. Energy Mater.*, 2022, **5**, 3677–3688.

63 J. H. Jung, C. W. Kang and S. U. Son, Cu Nanowire@Microporous Organic Polymer with Hydroquinones: Pseudocapacitive Materials with High Rate Performance, *ACS Appl. Energy Mater.*, 2022, **5**, 13149–13154.

64 K. Tian, J. Wang, L. Cao, W. Yang, W. Guo, S. Liu, W. Li, F. Wang, X. Li, Z. Xu, Z. Wang, H. Wang and Y. Hou, Single-site pyrrolic-nitrogen-doped sp^2-hybridized carbon materials and their pseudocapacitance, *Nat. Commun.*, 2020, **11**, 3884, DOI: **10.1038/s41467-020-17727-y**.

65 X. Feng, Y. Bai, M. Liu, Y. Li, H. Yang, X. Wang and C. Wu, Untangling the respective effects of heteroatom-doped carbon materials in batteries, supercapacitors and the ORR to design high performance materials, *Energy Environ. Sci.*, 2021, **14**, 2036–2089.

66 F. Rafik, H. Gualous, R. Gallay, A. Crausaz and A. Berthon, Frequency, thermal and voltage supercapacitor characterization and modeling, *J. Power Sources*, 2007, **165**, 928–934.

67 L. Zheng, B. Tang, X. Dai, T. Xing, Y. Ouyang, Y. Wang, B. Chang, H. Shu and X. Wang, High-yield synthesis of N-rich polymer-derived porous carbon with nanorod-like structure and ultrahigh N-doped content for high-performance supercapacitors, *Chem. Eng. J.*, 2020, **399**, 125671.

68 M. Ejaz, M. G. Mohamed, Y. T. Chen, K. Zhang and S. W. Kuo, Porous carbon materials augmented with heteroatoms derived from hyperbranched biobased benzoxazine resins for enhanced CO_2 adsorption and exceptional supercapacitor Performance, *J. Energy Storage*, 2024, **78**, 110166.

69 M. G. Mohamed, S. U. Sharma, N.-Y. Liu, T. H. Mansoure, M. M. Samy, S. V. Chaganti, Y.-L. Chang, J.-T. Lee and S.-W. Kuo, Ultrastable covalent triazine organic framework based on anthracene moiety as platform for high-performance carbon dioxide adsorption and supercapacitors, *Int. J. Mol. Sci.*, 2022, **23**, 3174.

70 M. M. Samy, M. G. Mohamed, S. U. Sharma, S. V. Chaganti, J.-T. Lee and S.-W. Kuo, An Ultrastable Tetrabenzonaphthalene-Linked conjugated microporous polymer functioning as a high-performance electrode for supercapacitors, *J. Taiwan Inst. Chem. Eng.*, 2023, 104750.

71 M. G. Mohamed, S. V. Chaganti, M.-S. Li, M. M. Samy, S. U. Sharma, J.-T. Lee, M. H. Elsayed, H.-H. Chou and S.-W. Kuo, Ultrastable Porous Organic Polymers Containing Thianthrene and Pyrene Units as Organic Electrode Materials for Supercapacitors, *ACS Appl. Energy Mater.*, 2022, **5**, 6442–6452.

72 S. U. Sharma, M. H. Elsayed, I. M. A. Mekhemer, T. S. Meng, H. H. Chou, S. W. Kuo and M. G. Mohamed, Rational design of pyrene and thienyltriazine-based conjugated microporous polymers for high-performance energy storage and visible-light photocatalytic hydrogen evolution from water, *Giant*, 2024, **17**, 100217.